Inorganic Chemistry

Article

pubs.acs.org/IC

Magnetic Mn and Co Complexes with a Large Polycyclic Aromatic Substituted Nitronylnitroxide

Maria G. F. Vaz,*[,†] Rafael A. Allão,[†] Handan Akpinar,[‡] John A. Schlueter,[§] Sauli Santos, Jr.,[⊥] Paul M. Lahti,*[,‡] and Miguel A. Novak[∥]

[†]Instituto de Química, Universidade Federal Fluminense, Niterói, RJ 24020-150, Brazil

[‡]Department of Chemistry, University of Massachusetts, Amherst, Massachusetts 01003, United States

[§]Materials Science Division, Argonne National Laboratory, Argonne, Illinois 60439, United States

[⊥]Curso de Física, Universidade Federal de Goiás, Jataí, GO 75804-120, Brazil

[∥]Instituto de Física, Universidade Federal do Rio de Janeiro, Rio de Janeiro, RJ 21941-972, Brazil

Supporting Information

ABSTRACT: 2-(1′-Pyrenyl)-4,4,5,5-tetramethyl-4,5-dihydro-1*H*-imidazole-3-oxide-1-oxyl (PyrNN) was reacted with $M(hfac)_2$ (M = Mn(II) and Co(II), hfac = hexafluoracetylacetonate) to give two isostructural ML_2 stoichiometry $M(hfac)_2(PyrNN)_2$ complexes and a ML stoichiometry one-dimensional (1-D) polymer chain complex $[Mn(hfac)_2(PyrNN)]$. The ML_2 complexes have similar crystal structures with monoclinic unit cells, in which one NO unit from each PyrNN ligand is bonded to the transition metal on cis vertices of a distorted octahedron. The major magnetic interactions are intracomplex metal-to-radical exchange (J), and intermolecular exchange across a close contact between the uncoordinated NO units (J'). For M = Mn(II) an approximate chain model fit gives g = 2.0, J = (−)125 cm^{-1} and J' = (−)49 cm^{-1}; for M = Co(II), g = 2.4, J = (−)180 cm^{-1}, and J' = (−)70 cm^{-1}. Hybrid density functional theory (DFT) computations modeling the intermolecular exchange by using only the radical units across the close contact are in good accord with the estimated values of J'. The chain type complex structure shows solvent incorporation for overall structure $[Mn(hfac)_2(PyrNN)]_n \cdot 0.5(CHCl_3) \cdot 0.5(C_7H_{16})$. Both NO groups of the PyrNN ligand are complexed to form helical chains, with very strong metal to radical antiferromagnetic exchange that gives overall ferrimagnetic behavior.

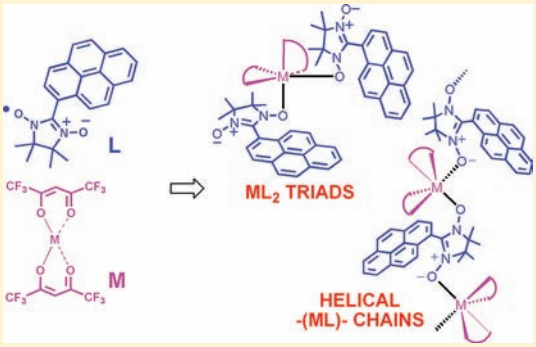

INTRODUCTION

The syntheses of molecular-based magnetic materials have been the object of increasing interest in the past years, in part because they may eventually be exploited in devices by molecular-electronics.[1] The combination of paramagnetic organic molecules with transition metals in complexes give rise to a wide variety of compounds with different crystalline structures and magnetic properties, through the so-called metal-radical strategy.[2] Among the organic paramagnetic molecules, nitroxide, verdazyl, and semiquinone radicals have been used extensively.[3] In particular, nitronylnitroxide derivatives (Chart 1) are one of the most explored in this strategy.[4] Nitronylnitroxide radicals can be made with a wide variety of structural units attached at the 2-position, and are generally stable. Although there is seldom more than a few percent of total spin density on the 2-position substituent groups, one or both of the high spin density N−O groups can be coordinated by the transition metals into clusters, chains, and higher dimensionality networks.[5]

Large aromatic rings have seen only limited use as the 2-substituents on nitronylnitroxides.[6,7] The use of such flat, disk shaped aromatics as part of ligating radicals may allow unusual crystal packing such as geometrically special helix formation or extended π-stacking, depending on the conformational flexibility of the attachment. They also may give prospects for new photochemical or photophysical behavior, when the aromatic unit is a strong light absorber. In this work we describe new molecular magnetic compounds made by reacting 2-(1′-pyrenyl)-4,4,5,5-tetramethyl-4,5-dihydro-1*H*-imidazole-3-oxide-1-oxyl (PyrNN) with $M(hfac)_2$ (M = Mn, Co; hfac = hexafluoracetylacetonate). Two molecular complexes with 1:2 metal:radical stoichiometry were obtained, $[M(hfac)_2(PyrNN)_2]$, as well as a 1:1 stoichiometry one-dimensional (1-D) polymer chain complex with manganese(II)—$[Mn(hfac)_2(PyrNN)]$—that has solvent incorporation into the structure. The molecular and crystal structures for these complexes are described below and related to their bulk magnetic properties. Some properties of PyrNN alone have been briefly described in the literature,[7,8] but to our knowledge this is the first time that any coordination complexes with it are described.

Received: December 5, 2011
Published: February 22, 2012

   dx.doi.org/10.1021/ic202623p | *Inorg. Chem.* 2012, 51, 3138−3145

Chart 1

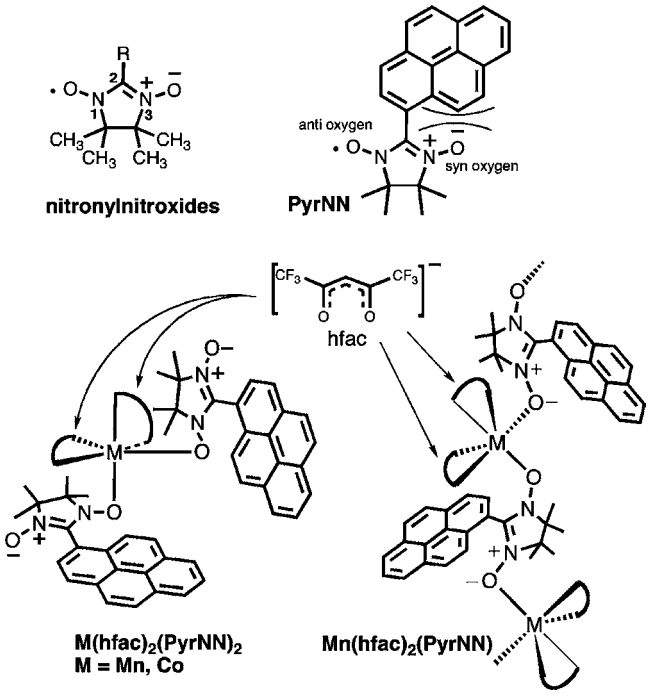

EXPERIMENTAL SECTION

General Procedures. All reagents and solvents were purchased from commercial sources and used without purification. Elemental analyses for the complexes were performed with a Perkin-Elmer CHN 2400 analyzer. Melting points are uncorrected.

Synthesis. *PyrNN.* This radical was made by condensation of 2,3-bis(hydroxylamino)-2,3-dimethylbutane hydrogensulfate[9] with 1-pyrenylcarboxaldehyde to get the bis(hydroxylamino) precursor, which was then dissolved in dichloromethane and oxidized with aqueous $NaIO_4$ at ice bath temperature, the layers separated, the organic solvent layer evaporated, the solid residue chromatographed (silica gel, ethyl acetate) and isolated by evaporation to yield the stable, deep blue radical as needles, typically in about 40% purified yield. Mp 190−191 °C. EPR (toluene, 9.65 GHz): 7.2 gauss (2 N). MS (FAB): Calc for $C_{23}H_{21}N_2O_2$ m/z = 357.2, found m/z = 357.2.

[M(hfac)$_2$(PyrNN)$_2$] where M = Mn(II) or Co(II), (1) and (2). To a solution of 0.050 g (9×10^{-5} mol) of $[M(hfac)_2]\cdot nH_2O$ dissolved in 25 mL of hot *n*-heptane, a solution of 0.065 g (18×10^{-5} mol) of PyrNN in 2 mL of chloroform was added under stirring. The mixture was heated at reflux for 20 min, then placed in a refrigerator. After 5 days, dark-green single-crystals were obtained. Anal. Calc. for $C_{56}H_{44}F_{12}N_4O_8Mn$ (**1**): C 56.81%, H 3.75%, N 4.73%. Found: C 57.16%, H 3.61%, N 4.77%. Anal. Calc. for $C_{56}H_{44}F_{12}N_4O_8Co$ (**2**): C 56.62%, H 3.73%, N 4.72%. Found: C 56.02%, H 3.71%, N 4.85%.

[Mn(hfac)$_2$(PyrNN)]·0.5(CHCl$_3$)·0.5(C$_7$H$_{16}$) (3). To a solution of $[M(hfac)_2]\cdot nH_2O$ 0.050 g (9×10^{-5} mol) dissolved in 25 mL of hot, anhydrous *n*-heptane, a solution of 0.033 g (9×10^{-5} mol) of PyrNN in 2 mL of chloroform was added while stirring. The mixture was heated at reflux for 30 min. The solution was then placed in a refrigerator. After 2 days, dark single-crystals were obtained. Anal. Calc. For $C_{37}H_{31.5}Cl_{1.5}MnF_{12}N_2O_6$ (**3**) C 47.47%, H 3.39%, N 2.99%. Found: C 47.31%, H 2.77%, N 2.73%. Crystallographic analyses show that (**3**) can lose entrained solvent molecules upon standing, sometimes with decomposition.

Magnetic Measurements. Magnetic measurements were performed on a Quantum Design MPMS SQUID magnetometer in the temperature range 2−300 K. The powder sample was placed in a gelatin capsule, and the magnetic data were corrected for the contribution of the sample holder. The sample diamagnetism correction was estimated from Pascal's constants.[10]

Crystallographic Procedures. Single crystal X-ray diffraction data for (**1**) and (**2**) were collected on Bruker-Kappa-CCD and Nonius Kappa-CCD diffractometers, respectively, using graphite-monochromated MoK_α radiation (λ = 0.71073 Å) at room temperature. Compound (**2**) crystallizes as poorer quality single-crystals that preclude a high quality result with crystal data refinement, but sufficient to show definitively that it is isostructural to compound (**1**). Final unit cell parameters were based on the fitting of the positions of all reflections using Collect.[11] Data integration and scaling of the reflections were performed with the HKL Scalepack.[12] Empirical multiscan absorption corrections using equivalent reflections were performed with the program Sortav.[13] The structures of compounds were solved by direct methods using the SHELXS program, and the refinement was performed using SHELXL based on F^2 through full-matrix least-squares routine.[14] All non-hydrogen atoms were refined with anisotropic displacement parameters. Hydrogen atoms were placed in calculated positions and refined isotropically using a riding model. Because of a large conformational disorder and to thermal motion present in the $-CF_3$ group, large thermal displacement parameters were found for these atoms. Nevertheless, this did not significantly affect the precision of the structural determination. The isotropic displacement parameters of all disordered atoms were freely refined.

The small size and delicate nature of the crystals of (**3**) did not permit its structure characterization using a conventional diffractometer. Data collection and structure determination were carried out at the 15ID ChemMatCARS beamline of the Advanced Photon Source, Argonne National Laboratory. The data were collected at 100 K with a Bruker 6000 CCD detector. Crystal structure and refinement data for compounds (**1**), (**2**), and (**3**) are summarized in Table 1.

RESULTS AND DISCUSSION

Crystallography. Compound (**1**) crystallizes in the centrosymmetric monoclinic *C*2/*c* space group. It consists of one manganese(II) ion located on 2-fold rotation axis with two hfac ligands and two PyrNN radicals, giving a somewhat distorted octahedral geometry with all six vertices occupied by oxygen atoms, four (O1, O2, O1^i, and O2^i) from the hfac ligands and two (O3 and O3^i) from the PyrNN radicals. Each PyrNN radical also has one nitronylnitroxide oxygen atom (O4) that is not coordinated (Figure 1). The ligand sphere bond lengths and angles are close to values previously reported for manganese(II)-nitronylnitroxide complexes.[15]

The closest contact between the noncoordinated oxygen atoms of the PyrNN nitronylnitroxide groups is r-[O(4)···O(4)^{ii}] = 3.374 Å. The set of intra- and intermolecular contacts forms an alternating pseudochain of transition metal and organic radical spin units that runs along the crystallographic *c* axis direction; an example is shown in Figure 2. Other close contacts occur between CH_3 groups of the PyrNN and O4 atom along the same chain contacts, namely, C20^{ii}···O4 = 3.359 Å, C23^{ii}···O4 = 3.388 Å.

Compound (**2**) is isostructural to (**1**); however, a smaller M−L bond length was observed for (**2**), as expected because the ionic radius of the metal decreases as the atomic number increases from manganese(II) to cobalt(II). An ORTEP diagram for (**2**) is shown in the Supporting Information, Figure S1; selected bond lengths and angles are given in Table 2. The ligand sphere bond lengths and angles are close to values previously reported for cobalt(II)-nitronylnitroxide complexes.[16] The intermolecular closest contact between the noncoordinated oxygen atoms of the PyrNN nitronylnitroxide groups (r[O(4)···O^{ii}(4)] = 3.462 Å) is slightly larger than in (**1**). Other close contacts like those in (**1**) also occur between CH_3 groups of the PyrNN and O4 atoms (see Supporting Information, Figure S2), as in (**1**). The set of intra- and intermolecular contacts forms an alternating pseudochain of

dx.doi.org/10.1021/ic202623p | Inorg. Chem. 2012, 51, 3138−3145

Table 1. Crystal Data and Structure Refinement for $[Mn(hfac)_2(PyrNN)_2]$ (1), $[Co(hfac)_2(PyrNN)_2]$ (2), and $[Mn(hfac)_2(PyrNN)]\cdot 0.16(CHCl_3)\cdot 0.5(C_7H_{16})$ (3)

identification	(1)	(2)	(3)
formula	$C_{56}H_{44}N_4O_8F_{12}Mn$	$C_{56}H_{44}N_4O_8F_{12}Co$	$C_{36.66}H_{31.16}N_2O_6F_{12}Cl_{0.48}Mn$
Fw (g mol^{-1})	1183.9	1187.88	895.70
T (K)	293(2)	100(2)	100
λ (Å)	0.71073	0.71073	0.4859
crystal system	monoclinic	monoclinic	monoclinic
space group	$C2/c$	$C2/c$	$P21/c$
a (Å)	24.2086(5)	24.193(6)	11.3999(17)
b (Å)	11.2969(3)	11.288(3)	13.8208(19)
c (Å)	22.9083(5)	22.682(8)	25.309(4)
β (deg)	120.411(2)	121.781(12)	99.904(2)
volume (Å^3)	5403.0(2)	5266(3)	3928.2(10)
Z	4	4	4
ρ_{calc} (Mg cm^{-3})	1.455	1.498	1.515
μ (mm^{-1})	0.344	0.428	0.124
$F(000)$	2420	2428	1817
θ range (deg)	4.10−25.00.	3.15−25.00	1.63−21.87
index ranges	$-28 \le h \le 28$	$-28 \le h \le 28$	$-10 \le h \le 10$
	$-13 \le k \le 13$	$-12 \le k \le 13$	$-12 \le k \le 12$
	$-27 \le l \le 27$	$-26 \le l \le 26$	$-23 \le l \le 23$
data collected	8088	8322	35746
independent reflections	4721 [R_{int} = 0.0145]	4510 [R_{int} = 0.01424]	3027 [R_{int} = 0.0934]
refinement method		full-matrix least-squares on F^2	
data/restraints/parameters	4721/0/422	4510/0/367	3027/106/574
GOF on F^2	1.024	1.045	1.011
R1,wR2 [$I > 2\sigma(I)$]	0.0405, 0.1066	0.1085, 0.2603	0. 1009, 0.2339
R1,wR2 (all)	0.0513, 0.1177	0.2579, 0.3077	0.1270, 0.2458
$\Delta\rho_{max}$, $\Delta\rho_{min}$ (e·Å^{-3})	0.163 and −0.168	0.413 and −0.346	1.48 and −0.76

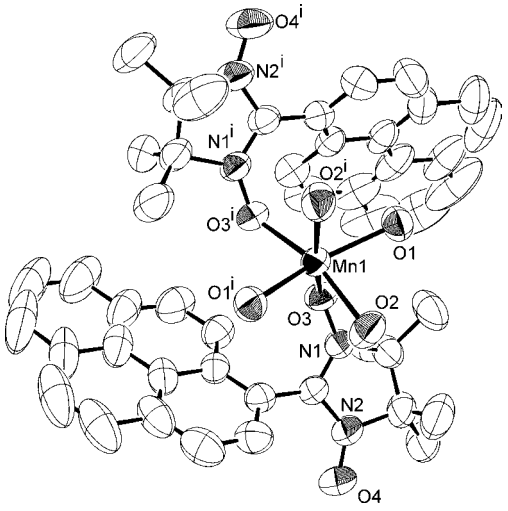

Figure 1. ORTEP view of the structure of compound (**1**) with ADPs at 50% probability. For clarity, carbon and fluorine atoms of hfac groups and hydrogen atoms were omitted.

transition metal and organic radical spin units along the crystallographic c axis direction, analogous to those found in (**1**).

Compound (**3**) crystallizes in the $P2_1/n$ space group with one independent manganese(II) ion and one PyrNN radical per unit cell. The manganese(II) ion is in a somewhat distorted octahedral environment, coordinated by four oxygen atoms (O1, O2, O3, and O4) from two hfac ligands, plus two oxygen (O5 and O6) atoms from cis-coordinated PyrNN radicals. Overall, the manganese(II) ions are bridged by PyrNN ligands to form helical chains having a 2_1 symmetry axis passing through the metal ion, parallel to the b axis (Figure 3). The intrachain metal−metal distance is 7.439 Å, while the closest interchain Mn−Mn distance is 11.400 Å. Thus, any magnetic exchange interactions between the metal ions must be mediated through the nitronylnitroxide units along the chains. The solvating n-heptane and chloroform molecules occupy what would otherwise be void space, contributing to a large interchain distance. An analysis involving virtual removal of the solvates and a search for void spaces large enough to hold an imaginary spherical probe of 1.2 Å radius finds 15% void volume in the structure of (**3**) (Supporting Information, Figure S3); a similar test of the structure of (**1**) gives zero analogous void volume. The solvate molecules thus appear to be important contributors to the ability of PyrNN to crystallize into the helical chain structure of (**3**), since otherwise the chains could not pack into a stable lattice without large voids. The solvate molecules desorb gradually, based on the observation that different crystals of (**3**) give different amounts of $CHCl_3$ occupancy. The loss of solvate causes samples of the chain complex gradually to degrade in crystallographic quality, and even physically to disintegrate under some conditions.

No major differences were found in the manganese(II) environments between compounds (**1**) and (**3**), as shown by comparison of analogous structural parameters in Table 2. Consequently the difference observed in their magnetic behaviors is attributed mainly to different coordination modes of the nitronylnitroxide radical. In fact, in the compound (**1**) an alternating magnetic pseudochain develops through intramolecular metal-radical magnetic interactions between manganese(II) and radical plus radical−radical intermolecular interactions between nitronylnitroxide moieties, as is discussed below. On the

dx.doi.org/10.1021/ic202623p | Inorg. Chem. 2012, 51, 3138−3145

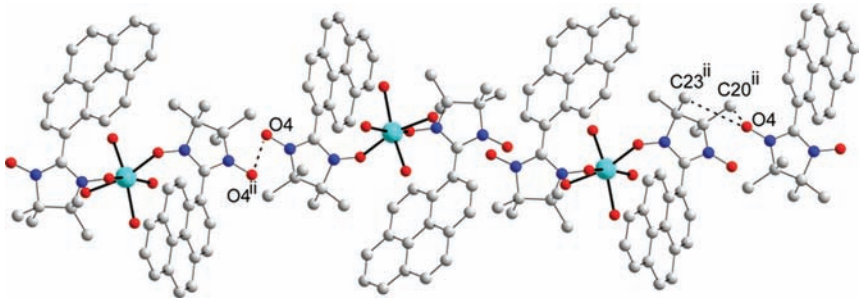

Figure 2. View of the pseudochain propagation along the crystallographic *c* direction in compound (**1**). (*ii* = 2−*x*, 1−*y*, 1−*z*). Carbon (gray), nitrogen (blue), oxygen (red), and manganese(II) (cyan) atoms are shown. For clarity, carbon and fluorine atoms of hfac groups and hydrogen atoms were omitted.

Table 2. Selected Bond Lengths (Å) and Angles (deg) for (1), (2), and (3)[a]

(1)		(2)		(3)	
		Bond Lengths			
Mn1−O1	2.1641(33)	Co−O1	2.081(7)	Mn1−O1	2.149(10)
Mn1−O2	2.1931(15)	Co−O2	2.054(6)	Mn1−O2	2.140(9)
Mn1−O3	2.1101(13)	Co−O3	2.047(7)	Mn1−O3	2.156(8)
				Mn1−O4	2.141(10)
				Mn1−O5	2.099(8)
				Mn1−O6^{iii}	2.106(8)
		Bond Angles			
O1−Mn1−O1^{i}	153.34(9)	O1^{i}−Co−O1	92.0(4)	O2−Mn1−O1	80.5(4)
O1−Mn1−O2	82.22(6)	O1−Co−O2	85.3(2)	O3−Mn1−O1	82.3(3)
O1^{i}−Mn1−O2	80.02(6)	O2−Co−O1^{i}	83.6(2)	O4−Mn1−O1	156.3(4)
O2−Mn1−O2^{i}	95.94(9)	O2−Co−O2^{i}	164.0(4)	O5−Mn1−O1	107.7(3)
O3− Mn1−O1	89.00(5)	O3− Co−O1	94.7(3)	O6^{iii}−Mn1−O1	104.8(3)
O3^{i}−Mn1−O1	111.57(6)	O3−Co−O1^{i}	171.2(3)	O3−Mn1−O2	97.7(4)
O3−Mn1−O2	93.00(6)	O3−Co−O2	102.6(2)	O4−Mn1−O2	84.1(4)
O3^{i}−Mn1−O2	164.74(6)	O3^{i}−Co−O2	89.8(2)	O5−Mn1−O2	89.6(4)
O3^{i}−Mn1−O3	81.14(7)	O3−Co−O3^{i}	79.2(4)	O6^{iii}−Mn1−O2	167.2(4)
Mn1−O3−N1	124.89(12)	Co−O3−N1	122.8(6)	O4−Mn1−O3	81.9(3)
				O5−Mn1−O3	168.6(3)
				O6^{iii}−Mn1−O3	92.4(4)
				O5−Mn1−O4	90.1(3)
				O6^{iii}−Mn1−O4	105.2(4)
				O6^{iii}−Mn1−O5	81.8(6)
				Mn1−O5−N1	126.7(6)
				Mn1−O6−N2^{iv}	123.0(7)

[a]Symmetry operations used to generate equivalent atoms: *i* = (2−*x*, *y*, 1/2−*z*), *iii* = (1−*x*, 1/2+*y*, 0.5−*z*); *iv* = (1−*x*, −1/2+*y*, 1/2−*z*).

other hand, in compound (**3**) the manganese(II) ions are bridged by nitronylnitroxide radicals, consequently its magnetic interactions are propagated by metal-radical pathways only.

Magnetic Properties. The temperature dependence of the susceptibility as χT for (**1**) is shown in Figure 4. At 300 K, χT is 2.10 cm^3 K mol^{-1}, much lower than expected (5.13 cm^3 K mol^{-1}) for noninteracting spin units, two nitronylnitroxide radicals and one manganese(II) ion with g = 2.00. This indicates the existence of strong intramolecular antiferromagnetic (AFM) exchange coupling between manganese(II) ion and the nitronylnitroxide radicals. When the temperature is decreased, χT shows a gradual decrease until 100 K followed by faster decrease to 0.09 cm^3 K mol^{-1} at 1.8 K. The additional, stronger decrease at lower temperature is attributable to the effects of *inter*molecular AFM interactions.

The crystal structure of (**1**) indicates that the major exchange interaction interactions should come from intrachain direct bonding between the PyrNN and Mn(1). Since all the d-orbitals of high spin manganese(II) are magnetically active, all typically are expected to spin-pair in AFM fashion by direct overlap with the nitronylnitroxide at the radical's large spin density N1−O3 π-symmetry singly occupied molecular orbitals (SOMO). The short *inter*molecular O(4)···O(4)^{ii} contacts between the uncoordinated N2−O4 radical units of the trimer complexes shown in Figure 2 form an excellent geometry for SOMO−SOMO overlap at the oxygen ends of the N2−O4 bonds, quite consistent with the observed AFM exchange.

An analytical expression appropriate to describe the magnetic behavior according to a chain with spin topology $-J_a-J_a-J_b-$ was not found in the literature; therefore, as a first attempt the χT versus T data were fit to a linear isotropic three spin model[17] with the Hamiltonian $H = -J_a(S_{Mn}\cdot S_{Rad}+S_{Mn}\cdot S_{Rad})$ where S_{rad} = 1/2 and S_{Mn} = 5/2. Besides the intratrimer coupling, J_a, an inter-trimer magnetic interaction, J_b, was used to account for the intermolecular O(4)···O(4)^{ii} contact between PyrNN radicals. The weak inter-trimer magnetic interaction was treated as mean field correction,[18] following the manner used by others to model similar alternating one-dimensional pseudochains of trimers.[19]

dx.doi.org/10.1021/ic202623p | *Inorg. Chem.* 2012, 51, 3138−3145

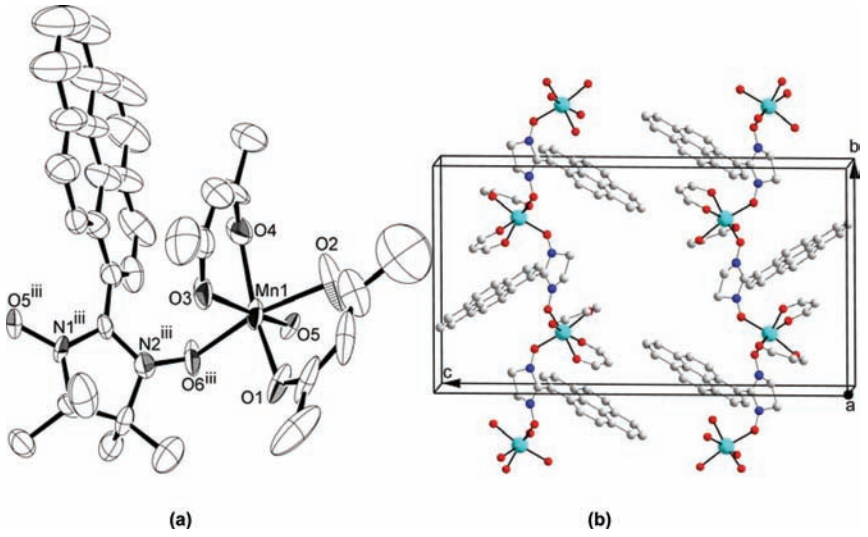

Figure 3. (a) ORTEP style representation of (**3**), with APDs at 50% probability. All solvent molecules, hydrogen, and fluorine atoms are omitted for clarity. (b) View of the chain propagation along the crystallographic ***b*** direction in (**3**), with solvent molecules hydrogen atoms, methyl, and CF_3 groups omitted for clarity. Carbon (gray), nitrogen (blue), oxygen (red), and manganese(II) (cyan) atoms are shown.

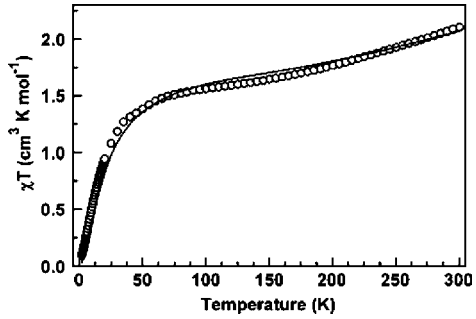

Figure 4. Temperature dependence of the product (χT) of (**1**) at 1000 Oe. The black line was obtained by simulation using the model of Figure 5 described in the text.

The magnetic susceptibility data were fairly well reproduced by this approximation with the best fit parameters $g = 2.00$ (fixed), $J_a = -169$ cm^{-1}, $zJ_b = -0.6$ cm^{-1}, where $z = 2$ in our case (see Supporting Information, Figure S4). However, this approximation has limitations, because it is an oversimplification that is most valid for low dimensional magnetism of well isolated trimers. Despite the fairly good quality of the fit, the expected exchange coupling due to the intermolecular magnetic interaction seems very unlikely to be so low because of the close contact. For example, moderate antiferromagnetic interactions in the absolute range (20−55) cm^{-1} were observed between isolated neighboring nitronylnitroxide molecules with similar geometries to the SOMO−SOMO overlap of the oxygen atoms of nitroxide groups in (**1**) and (**2**).[20] As is described in the next section, modeling the radical−radical only interaction based on the intercomplex geometry also gives an expectation of significant intermolecular exchange.

To obtain a more realistic description of the magnetic behavior, the magnetic data were analyzed considering a full chain topology approximate model. The susceptibility versus temperature behavior was simulated using the MAGPACK package software[21] assuming a finite twelve-membered ring with the spin site pattern outlined in Figure 5; this model was the largest approximation to a chain that was possible within program limitations.

A reasonable fit to the experimental data (solid black line in Figure 4) was found for $g = 2.00$, $J = -125$ cm,$^{-1}$ and $J' = -49$ cm^{-1}.

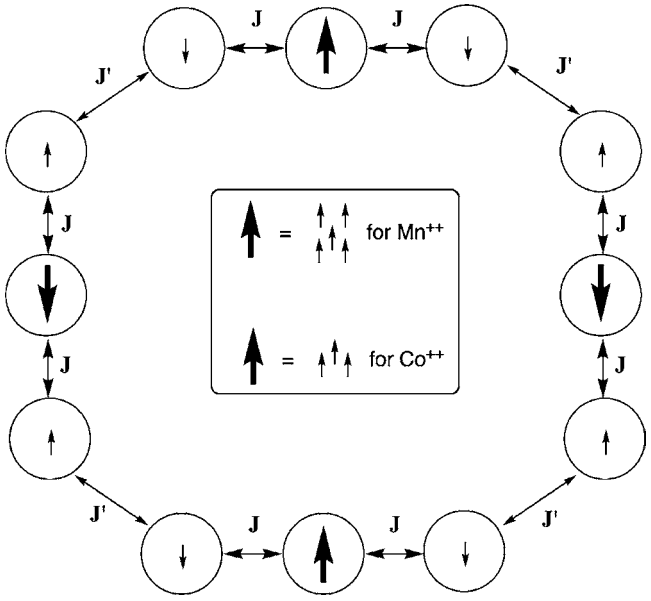

Figure 5. Spin topology model used to simulate magnetic susceptibility behavior of (**1**) and (**2**).

The shape of the experimental curve is not well reproduced with values of the two exchange constants that vary by <5−10 cm^{-1}. These results are in good agreement with the strong intramolecular AFM exchange expected for a manganese(II)-nitroxide radical bond, and the expectation of significant intermolecular exchange.[22] Of course, one must keep in mind the limitations of using a modest sized finite model to approximate a chain system.

Compound (**2**) is isostructural to (**1**) and similar magnetic behavior was observed (Figure 6). Therefore, the ring model of Figure 5 was also used to approximate the behavior of (**2**), albeit with the same limitations as for its use with (**1**), and additional complications from the Kramers behavior of cobalt(II). Using a spin only approximation for the tetrad of trimers with MAGPACK, a reasonably good simulation of the χT versus T data was achieved using $g = 2.4$, $J = -180$ cm^{-1}, $J' = -70$ cm^{-1}; the simulated curve is shown in Figure 6. Despite

dx.doi.org/10.1021/ic202623p | Inorg. Chem. 2012, 51, 3138−3145

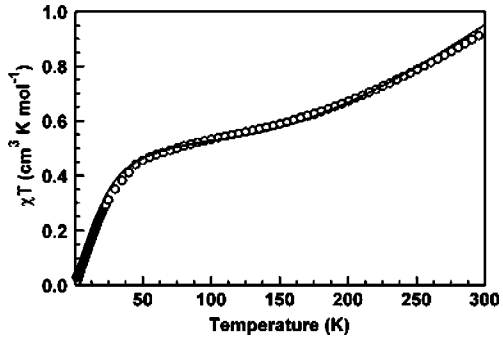

Figure 6. Temperature dependence of the product (χT) of (**2**) at 1000 Oe. The black line is the simulation for the model of Figure 5 described in the text.

the crystal structure similarity between (**1**) and (**2**), larger values of J and J' were observed for (**2**), as is usually found in comparing the magnetic behaviors of isostructural manganese(II) and cobalt(II) coordination compounds.[23]

An estimate of the intertrimer exchange coupling was made by density functional theory (DFT) calculation, using a radical-contact only approximation. A close-contact pair of molecules from the crystal structure of (**1**) was truncated by removing both $Mn(hfac)_2$ units; the two pyrenyl units were then replaced by hydrogen atoms, and the geometry of the resultant model radical pair was frozen. This model ignores potential effects of coordination on the spin densities of the nitronylnitroxide groups, but still should allow a reasonable estimate of whether the intermolecular exchange is fairly strong or not. Both $S = 1$ and $S = 0$ states were computed using UB3LYP[24]/6-31G* and UB97D[25]/6-31+G(d) functions in Gaussians09;[26] the latter uses Grimme's dispersion-corrected functional. For both methods, the $S = 0$ state was modeled with a broken symmetry, unrestricted wave function. No zero point energy corrections were applied. Singlet to triplet exchange energy gaps were corrected for spin contamination in the broken symmetry wave function using Yamaguchi's[27] method. By the UB3LYP method, $\Delta E_{T\text{-}S} = -58$ cm^{-1}, by the UB97D method, $\Delta E_{T\text{-}S} = -96$ cm^{-1}; in both cases, the negative number means an antiferromagnetic exchange interaction. These values are in reasonable accord with the estimates made using the cluster model of Figure 5.

The temperature dependence of χT for the chain system (**3**) is very different from those of the ML_2 systems, showing a strong increase with dropping temperature up to a maximum of $\chi T = 86$ cm^3 K mol^{-1} at 8.0 K and an external field of 1000 Oe. Below this temperature χT decreases quickly to 30 cm^3 K mol^{-1} at the lowest measured temperature of 1.8 K (Figure 7). A

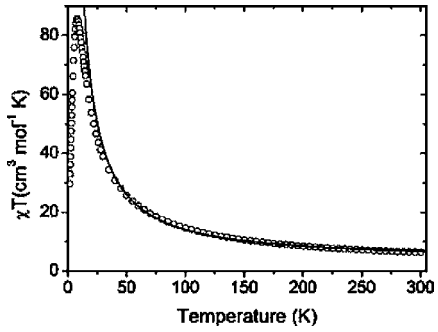

Figure 7. (a) Temperature dependence of the product of magnetic susceptibility and temperature (χT) for (**3**) at 1000 Oe. The solid line shows a fit to eq 1 to data above 40 K.

Curie–Weiss linear fit of the $1/\chi$ versus T data for (**3**) for $T >$ 225 K yields a Weiss constant of $\theta = +81$ cm^{-1} (Supporting Information, Figure S5).

Overall, the magnetic behavior of (**3**) is typical of monodimensional ferrimagnetic chains composed of manganese(II) ($S = 5/2$) and nitronylnitroxide radical ($S = 1/2$) spin units. Since no minimum in χT was observed in the measured temperature range as expected for a ferrimagnetic chain of this type, the metal to radical exchange interaction must be quite strong, at least -92 cm^{-1} judging by previous[28] examples ($H = -J\sum \boldsymbol{S}_i \cdot \boldsymbol{S}_{i+1}$). Since strong antiferromagnetic interactions were found for compounds (**1**) and (**2**) with their structurally similar manganese(II) to nitronylnitroxide coordination, strong exchange coupling can reasonably be expected for (**3**).

To obtain a more precise description of the magnetic properties of (**3**), its magnetic data were analyzed using Seiden's ferrimagnetic chain model[29] with the addition of a paramagnetic impurity of concentration ρ, given by eq 1. Here, the PyrNN $S_R = 1/2$ spin units are treated as quantum spins, and the transition metal spins $S_{Mn} = 5/2$ are treated classically. The Landé factor g_R for the radical was fixed at 2.00, and g_{Mn} was allowed to vary. A single exchange constant J was used with the Hamiltonian $H = -J_a\sum \boldsymbol{S}_i \cdot \boldsymbol{S}_{i+1}$, where S_i and S_{i+1} are always neighboring PyrNN and manganese(II) units. The other terms have the same meanings given earlier.

$$\chi T = \frac{N\mu_B^2}{3k}\left\{g_{Mn}^2 S_{Mn}^2\left(\frac{S_{Mn}+1}{S_{Mn}} + \frac{2\delta}{1-\delta}\right) - 4g_{Mn}g_R\Lambda S_R S_{Mn}\frac{1}{1-\delta} + g_R^2\left(S_R(S_R+1) + 2\Lambda^2 S_R^2\frac{1}{1-\delta}\right)\right\}$$

$$\gamma = -JS_{Mn}/kT$$

$$a_0 = 4(\gamma^{-1}\sinh\gamma - \gamma^{-2}\cosh\gamma + \gamma^{-2})$$

$$a_1 = 12[(\gamma^{-1} + 12\gamma^{-3})\sinh\gamma - (5\gamma^{-2} + 12\gamma^{-4})\cosh\gamma - \gamma^{-2} + 12\gamma^{-4})]$$

$$b_0 = \gamma^{-1}(\cosh\gamma - 1)$$

$$b_1 = 3[(\gamma^{-1} + 4\gamma^{-3})\cosh\gamma - 4\gamma^{-2}\sinh\gamma + \gamma^{-1} - 4\gamma^{-3})]$$

$$\delta = \frac{a_1}{3a_0},\ \Lambda = 2\left(\frac{b_1}{3a_0} + \frac{b_0}{a_0}\right) \quad (1)$$

dx.doi.org/10.1021/ic202623p | Inorg. Chem. 2012, 51, 3138–3145

The χT versus T data for (3) were fitted to the above conditions for data where $T > 40$ K. The fitted curve is shown in Figure 7, where $g_{Mn} = 2.24$, $\rho = 0.07$, $J = -1100 \pm 150$ cm^{-1}. This is higher than values previously reported for monodimensional Mn(II)-nitronylnitroxide radical ferrimagnetically coupled chains,[28,29b,30] but is not unreasonable given the challenge in fitting the large exchange constant. Using a single, fixed value of $g = 2.00$ and no fitted paramagnetic contribution for the same fit yields nearly the same value of J to within statistical uncertainty. Fitting the lower temperature data near the downturn in χT versus T is problematic because of saturation of the susceptibility at the maximum correlation length in the ferrimagnetically coupled chain. Because of this, the temperature of the χT maximum for (3) changes from 8 K at 1000 Oe to 3 K at 100 Oe (see Supporting Information, Figure S6). Seiden gives[29a] the correlation length $\xi = |J/2|\cdot S/4kT$, so for (3) $\xi = 43$ from the 1000 Oe χT maximum, and $\xi = 115$ from the 100 Oe maximum. The susceptibility nearly levels off at lower temperatures (Supporting Information, Figure S6) for χ versus T at both 100 and 1000 Oe; at higher temperatures the data follow a power law with an exponent of −1.82.

The analysis described above was somewhat challenging. Because of the strong interactions the temperature region where the spins behave isolated or even the minimum in χT were inaccessible. In addition samples of (3) sometimes decomposed to greater or lesser extents upon standing, because of the above-described solvate molecule desorption, introducing disorder in the chain and gave varying amounts of paramagnetic impurity. But, overall behavior was consistent with strong AFM exchange between manganese(II) and nitronylnitroxide units, giving ferrimagnetic chain formation resulting in magnetic susceptibilities well above the Curie isolated spin value. There was no evidence that (3) undergoes an ordering transition at temperatures above 2 K.

CONCLUSIONS

Coordination of PyrNN with manganese(II) and cobalt(II) dications yields isostructural ML_2 complexes having strongly antiferromagnetic metal to radical exchange at both metal to radical bonds. The ML_2 complexes form readily despite the large volume occupied by the polycyclic aromatic hydrocarbon substituent on PyrNN. Notably, $Mn(hfac)_2$ also yields a 1:1 stoichiometry $(ML)_n$ ferrimagnetic chain complex with PyrNN when the reactants are combined in some solvents. Solvent choice appears to be very important to allow chain formation by filling what would otherwise be void space. Numerous $(ML)_n$ chain complexes have been made with nitronylnitroxide ligands, but in virtually all cases with fairly small (typically substituted benzene) substituents on the nitronylnitroxide radical unit. The ability to make chains using such large substituents as pyrene on the radical unit offers a wide variety of opportunities for making new helical chain solids with photoactive or electroactive substituents radiating around the perimeter, especially if solvent variation can be used in analogous cases to encourage chain formation over simpler cluster formation.

ASSOCIATED CONTENT

Supporting Information

Crystallographic figures for compound (2), void space figure for crystallographic packing of (3), magnetic modeling of (1) with a linear three-spin plus mean-field model, Curie−Weiss plot of magnetic susceptibility for (3), temperature dependence of dc magnetic susceptibility of (3), crystallographic data for (1)−(3) in CIF format, archive data and full Gaussian09 citation for estimate of intermolecular exchange by the radical pair model. This material is available free of charge via the Internet at http://pubs.acs.org.

AUTHOR INFORMATION

Corresponding Author

*E-mail: mariavaz@vm.uff.br (M.G.F.V.), lahti@chem.umass.edu (P.M.L.).

Notes

The authors declare no competing financial interest.

ACKNOWLEDGMENTS

M.G.F.V. and M.A.N. thank the research grants (BEX 1195/10-7 and BEX 0924/10-5) from CAPES (Brazil). R.A.A. also acknowledges CAPES, and financial support from FAPERJ and CNPq (Brazil). H.A. and P.M.L. thank the National Science Foundation (U.S.A.) for support through Grant CHE-0809791, and for support to the University of Massachusetts Amherst Nanomagnetics Facility through Grant CTS-0116498. Use of the Advanced Photon Source was supported by the U.S. Department of Energy, Office of Science, Office of Basic Energy Sciences, under Contract No. DE-AC02-06CH11357. ChemMatCARS Sector 15 is principally supported by the National Science Foundation/Department of Energy under Grant NSF/CHE-0822838. The authors acknowledge Professor Javier Ellena for the allocation of beam time on a Nonius Kappa-CCD diffractometer and laboratory facilities.

REFERENCES

(1) (a) Gatteschi, D.; Coronado, E. *J. Mater. Chem.* **2006**, *16*, 2513. (b) Gaspard, A. B.; Munoz, M. C.; Real, J. A. *J. Mater. Chem.* **2006**, *16*, 2522.

(2) (a) Caneschi, A.; Gatteschi, D.; Sessoli, R.; Rey, P. *Acc. Chem. Res.* **1989**, *22*, 392. (b) Maspoch, D.; Domingo, N.; Ruiz-Molina, D.; Wurst, K.; Vaughan, G.; Tejada, J.; Rovira, C.; Veciana, J. *Angew. Chem., Int. Ed.* **2004**, *43*, 1828. (c) Numata, Y.; Inoue, K.; Baranov, N.; Kurmoo, M.; Kikuchi, K. *J. Am. Chem. Soc.* **2007**, *129*, 9902. (d) Souza, D. A.; Florencio, A. S.; Soriano, S. S.; Calvo, R.; Sartoris, R.; Carneiro, J.W. de M.; Sangregorio, C.; Novak, M. A.; Vaz, M. G. F. *Dalton Trans.* **2009**, 6816. (e) Allão, R. A.; Jordão, A. K.; Resende, J. A. L. C.; Cunha, A. C.; Ferreira, V. F.; Novak, M. A.; Sangregorio, C.; Sorace, L.; Vaz, M. G. F. *Dalton Trans.* **2011**, *40*, 10843.

(3) (a) Bencini, A.; Caneschi, A.; Dei, A.; Gatteschi, D.; Sangregorio, C.; Shultz, D.; Sorace, L.; Vaz, M. G. F. *C. R. Chim.* **2003**, *6*, 663. (b) Luneau, D.; Rey, P. *Coord. Chem. Rev.* **2005**, *249*, 2591. (c) Norel, L.; Pointillart, F.; Train, C.; Chamoreau, L.-M.; Boubekeur, K.; Journaux, Y.; Brieger, A.; Brook, D. J. R. *Inorg. Chem.* **2008**, *47*, 2396. (d) Baskett, M.; Paduan-Filho, A.; Oliveira, N. F.; Chandrasekaran, A.; Mague, J. T.; Lahti, P. M. *Inorg. Chem.* **2011**, *50*, 5060. (e) Evangelio, E.; Ruiz-Molina, D. *Eur. J. Inorg. Chem.* **2005**, 2957.

(4) Inoue, K. *Structure and Bonding*; Springer-Verlag: Berlin, Germany, 2001; Vol. *100*, p 61 ff.

(5) (a) Cador, O.; Vaz, M. G. F.; Mathoniere, C.; Stumpf, H. O. *J. Magn. Magn. Mater.* **2001**, *234*, 6. (b) Romanenko, G. V.; Maryunina, K. Y.; Sagdeev, R. Z.; Ovcharenko, V. I. *Inorg. Chem.* **2011**, *50*, 6597. (c) Luneau, D.; Borta, A.; Chumakov, Y.; Jacquot, J.-F.; Jeanneau, E.; Lescop, C.; Rey, P. *Inorg. Chim. Acta* **2008**, *361*, 3669. (d) Vaz, M. G. F.; Pinheiro, L. M. M.; Stumpf, H. O.; Alcantara, A. F. C.; Golhen, S.; Ouahab, L.; Cador, O.; Mathoniere, C.; Kahn, O. *Chem.—Eur. J.* **1999**, *5*, 1486.

(6) (a) Nishida, S.; Morita, Y.; Kobayashi, T.; Fukui, K.; Ueda, A.; Sato, K.; Shiomi, D.; Takui, T.; Nakasuji, K. *Polyhedron* **2005**, *24*, 2200. (b) Lozinsky, E.; Martin, V. V.; Berezina, T. A.; Shames, A. I.; Weis, A. L.; Likhtenshtein, G. I. *J. Biochem. Biophys. Methods* **1999**, *38*,

29. (c) Medvedeva, N.; Martin, V. V.; Weis, A. L.; Likhtenshten, G. I. *J. Photochem. Photobiol. A* **2004**, *163*, 45. (d) Lozinsky, E. M.; Martina, L. V.; Shames, A. I.; Uzlaner, N.; Masarwa, A.; Likhtenshtein, G. I.; Meyerstein, D.; Martin, V. V.; Priel, Z. *Anal. Biochem.* **2004**, *326*, 139. (e) Teki, Y.; Iimura, K.; Sato, M.; Fukuda, Y.; Miura, Y. *Mol. Cryst. Liq. Cryst. Sci. Tech. Sec. A.* **1999**, *334*, 305.

(7) (a) Wang, H.; Zhang, D.; Guo, X.; Zhu, L.; Shuai, Z.; Zhu, D. *Chem. Commun.* **2004**, 670. (b) Wang, Y.; Wang, H.; Liu, Y.; Di, C.; Sun, Y.; Wu, W.; Yu, G.; Zhang, D.; Zhu, D. *J. Am. Chem. Soc.* **2006**, *128*, 13058.

(8) Crystal structure of PyrNN was reported in Mann, C.; Gompper, R.; Polborn, K. 2003, CSD Code ENIZIK, CCDC Deposition #226038, private communication.

(9) Ovcharenko, V.; Fokin, S.; Rey, P. *Mol. Cryst. Liq. Cryst. Sect. A* **1999**, *334*, 109.

(10) Bain, G. A.; Berry, J. F. *J. Chem. Educ.* **2008**, *85*, 532.

(11) Hooft, R. W. W. *COLLECT*; Nonius BV: Delft, The Netherlands, 1998.

(12) Otwinowski, Z.; Minor, W. In *Methods in Enzymology: Macromolecular Crystallography, Part A*; Carter, C. W., Jr., Sweet, R. M., Eds.; Academic Press: New York, NY, 1997; Vol. *276*, pp 307–326.

(13) (a) Blessing, R. H. *Acta Crystallogr.* **1995**, *A51*, 33. (b) Blessing, R. H. *J. Appl. Crystallogr.* **1997**, *30*, 421.

(14) Sheldrick, G. M. *Acta Crystallogr.* **2008**, *A64*, 112.

(15) (a) Caneschi, A.; Gatteschi, D.; Lirzin, A. L. *J. Mater. Chem.* **1994**, *4*, 319. (b) Liu, Z. L.; Zhao, Q. H.; Li, S. Q.; Liao, D. Z.; Jiang, Z. H.; Yan, S. P. *Inorg. Chem. Commun.* **2001**, *4*, 322.

(16) (a) Koreneva, O. V.; Romanenko, G. V.; Shvedenkov, Y. G.; Ikorskii, V. N.; Ovcharenko, V. I. *Polyhedron* **2003**, *22*, 2487. (b) Caneschi, A.; Gatteschi, D.; Lalioti, N.; Sessoli, R.; Sorace, L.; Tangoulis, V.; Vindigni, A. *Chem.—Eur. J.* **2002**, *8*, 286.

(17) Kahn, O. *Molecular Magnetism*; Wiley-VCH: Weinheim, Germany, 1993.

(18) O'Connor, C. J. *Prog. Inorg. Chem.* **1982**, *29*, 203.

(19) (a) Biswas, A.; Drew, M. G. B.; Gómez-Garcia, C. J.; Ghosh, A. *Inorg. Chem.* **2010**, *49*, 8155. (b) Ma, Y.; When, Y. Q.; Zhang, J. Y.; Gao, E. Q.; Liu, C. M. *Dalton Trans.* **2010**, *39*, 1846.

(20) (a) Minguet, M.; Amabilino, D. B.; Vidal-Gancedo, J.; Wurst, K.; Veciana, J. *J. Mater. Chem.* **2002**, *12*, 570. (b) Awaga, K.; Yamaguchi, A.; Okuno, T.; Inabe, T.; Nakamura, T.; Matsumoto, M.; Maruyama, Y. *J. Mater. Chem.* **1994**, *4*, 1377.

(21) Borrás-Almenar, J. J.; Clemente-Juan, J. M.; Coronado, E.; Tsukerblat, B. S. *J. Comput. Chem.* **2001**, *22*, 985.

(22) (a) Dickman, M. H.; Porter, L. C.; Doedens, R. J. *Inorg. Chem.* **1986**, *25*, 2595. (b) Caneschi, A.; Gatteschi, D.; Laugier, J.; Pardi, L.; Rey, P.; Zanchini, C. *Inorg. Chem.* **1988**, *27*, 2027. (c) Iwahori, F.; Matsumura, K.; Yamashita, M.; Abe, J. *Chem. Lett.* **2006**, *35*, 68.

(23) (a) Sun, H. L.; Wang, Z. M.; Gao, S. *Chem.—Eur. J.* **2009**, *15*, 1757. (b) Coronado, E.; Giménez-Saiz, C.; Romero, F. M.; Tarazón, A. *Inorg. Chem.* **2009**, *48*, 2205. (c) Keene, T. D.; Zimmermann, I.; Neels, A.; Sereda, O.; Hauser, J.; Bonin, M.; Hursthouse, M. B.; Price, D. J.; Decurtins, S. *Dalton Trans.* **2010**, *39*, 4937.

(24) (a) Lee, C.; Yang, W.; Parr, R. G. *Phys. Rev. B* **1988**, *37*, 785. (b) Becke, A. D. *J. Chem. Phys.* **1993**, *98*, 5648. (c) Stephens, P. J.; Devlin, F. J.; Chabalowski, C. F.; Frisch, M. J. *J. Phys. Chem.* **1994**, *98*, 11623.

(25) Grimme, S. J. *J. Comput. Chem.* **2006**, *27*, 1787.

(26) Frisch, M. J.; et al. *Gaussian 09*, Revision B.01; Gaussian, Inc: Wallingford, CT, 2010. See the full citation in the Supporting Information.

(27) For a high spin state having energy E_{HS} and spin-squared expectation value $\langle S^2\rangle_{HS}$,, and a low spin state having E_{LS} and spin-squared expectation value $\langle S^2\rangle_{LS}$ the high spin to low spin energy gap $\Delta E_{HS\text{-}LS} = (E_{LS}-E_{HS})/\{\langle S^2\rangle_{HS} - \langle S^2\rangle_{LS}\}$. (a) Yamaguchi, K.; Fukui, H.; Fueno, T. *Chem. Lett.* **1986**, 625. (b) Yamaguchi, K. *Chem. Phys. Lett.* **1988**, *149*, 537.

(28) Caneschi, A.; Gatteschi, A.; Rey, P.; Sessoli, R. *Inorg. Chem.* **1988**, *27*, 1756.

(29) (a) Seiden, J. *J. Phys. Lett. (Paris)* **1983**, *44*, L–947. (b) The terminology of the equation that we used was also described in Ise, T.; Ishida, T.; Hashizume, D.; Iwasaki, F.; Nogami, T. *Inorg. Chem.* **2003**, *42*, 6106.

(30) Caneschi, A.; Gatteschi, D.; Lalioti, N.; Sangregorio, C.; Sessoli, R. *J. Chem. Soc., Dalton Trans.* **2000**, 3907.